True-Time Delay Line Based on Dispersion-Flattened 19-Core Photonic Crystal Fiber

Sabahat Shaheen [ORCID], Itandehui Gris-Sánchez, and Ivana Gasulla [ORCID], *Senior Member, IEEE*

Abstract—A novel design of a tunable True-Time delay line (TTDL) based on a multicore photonic crystal fiber (PCF) is proposed. It enables simultaneous transport and processing of microwave photonic signals over a broad radiofrequency processing range. Independent group delay behavior in 19 different cores characterized by a constant differential group delay between cores provides TTDL operation on 19 signal samples. The 19-core PCF structure allows tailoring the chromatic dispersion range between 1.5 and 31.2 ps/nm·km, which translates into a very broad microwave signal processing range from a few up to tens of GHz. A near-zero dispersion slope reduces the time delay errors in the TTDL's operation to less than 5% in a 40-nm optical wavelength range, thus ensuring its satisfactory performance. Its performance as a TTDL is evaluated in terms of higher-order dispersion as well as other degradation effects such as crosstalk and nonlinear fiber response. A high index contrast between core and cladding, between 0.3 to 1.5%, enables low intercore crosstalk and confinement losses as well as greater robustness against fiber bends and twists. Fabrication of this type of MCF might be possible although it will prove challenging. This work advances the state-of-the-art of a TTDL based on SDM technology by increasing the number of samples and microwave processing range.

Index Terms—Microwave photonics. multicore fibers, photonic crystal fibers, spatial division multiplexing.

I. INTRODUCTION

TRUE time Delay Line (TTDL) is a key element in many important microwave photonic (MWP) applications such as microwave signal filtering, optical beamforming for phase-array antennas, arbitrary waveform generation and multigigabit-per-second analog-to-digital conversion, amongst others [1]. As the core of time-discrete signal processing, the goal of the TTDL is to provide a set of different time-delayed samples that are characterized by a constant differential delay between them. Several solutions have been reported of optical TTDLs where the signal diversity is provided by either the space dimension (different path lengths) or the optical wavelength dimension (dispersive behavior of the optical medium). Fiber-based approaches include switched schemes with separate optical fibers and passive couplers [2], grating inscriptions [3], [4], or even nonlinear effects [5]. Nevertheless, none of these solutions provide in a single optical fiber both space and optical wavelength diversity operation modes.

The current interest in optical space division multiplexing (SDM), fueled by a need for higher transmission capacities, has motivated further the development of novel multicore optical fibers (MCFs) [6]. SDM finds a natural application in optical fiber-based TTDLs as the bulk of optical fibers can now be gathered in a single strand [7] with a considerable reduction in size and weight. Furthermore, thanks to the combination of space and optical wavelength dimensions, SDM-based TTDLs offer a higher degree of versatility and flexibility. Several SDM fiber technologies have been previously proposed and demonstrated as distributed signal processing solutions, where each individual spatially multiplexed path provides a given TTDL sample. These spatial paths can either be individual homogeneous [8] or heterogeneous cores of a MCF [9], [10], or individual modes in a few-mode fiber [11].

While each of the above mentioned SDM technologies brings distinct advantages depending on the application scenario [12], the use of Photonic Crystal Fibers (PCFs) [13], unexplored so far with reference to SDM-based TTDLs, can bring several advantages over solid-core designs. To begin with, PCFs can offer greater robustness against bend-induced losses due to the possibility of higher index contrast between core and cladding [14], [15]. The stacking mechanism used for PCF fabrication is well suited for multicore designs [15], [16]. Moreover, a single preform can potentially be used to draw multiple different cores, thus reducing sources of error and enabling simpler and less costly fabrication [16]. Most importantly, not only is it possible to vary the chromatic dispersion of a PCF over a broad range of values but, also, its dispersion slope can be made near-zero or invariant over a given range of wavelengths [14], [17]. These features address key requirements of a TTDL design where a broad range of dispersion values, preferably starting at zero or low values, implies greater radio frequency processing range [7]. Whereas, a near-zero dispersion slope (also called flat dispersion), reduces errors in the TTDL performance related to higher-order dispersion [7]. This requirement of zero and flat-dispersion has been pursued intensively in the development of PCFs for transmission applications: One of the earliest zero-
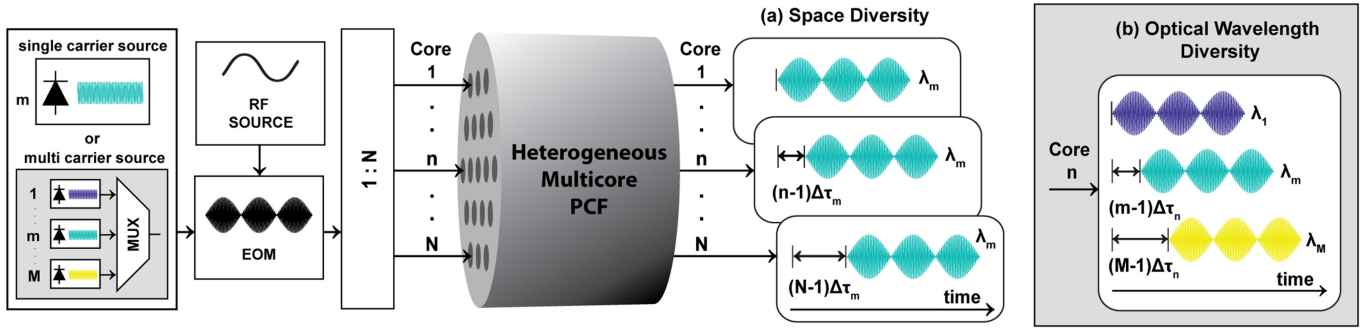
Fig. 1. Heterogeneous multicore PCF as a sampled delay line, fed by an RF modulated single- or multi-carrier optical source. (a) Single-carrier source: At the output, each core incurs an independent group delay to the input signal such that the differential group delay, $\Delta\tau$, is common to all cores. (b) Multi-carrier source: In addition to the space diversity, the exploitation of wavelength diversity allows another set of delay lines characterized by a constant differential group delay $\Delta\tau_n$ between consecutive carriers within each core n. RF: radiofrequency; EOM: Eletro-optic modulator.

and flat-dispersion designs comprised only three rings of air-holes [18], but, in practice, eleven rings were required to control the confinement loss [19]. Later, variable airhole sizes for each ring were introduced to accommodate the total air fraction with smaller number of rings [20]. Several other flat and/or zero dispersion designs are relevant to our work [20]–[25].

In this work, we present, for the first time to our knowledge, a multicore PCF that operates as a fiber-distributed element for microwave signal processing. Section II provides the design of a heterogeneous 19-core PCF to act as a 19-sample TTDL fulfilling the pertinent requirements in terms of incremental group delay and chromatic dispersion properties. In Section III, we evaluate the performance of the designed TTDL in terms of the main sources of degradation. Finally, Section IV closes the paper with the relevant conclusions.

II. DESIGN OF MULTICORE PCF AS A TTDL

A. Requirements to Operate as a TTDL

A TTDL based on a MCF can work in two different operation regimes, space diversity and wavelength diversity, depending upon whether the TTDL samples are provided by the different fiber cores or by different input optical wavelengths, respectively [7]. The basic group delay τ_n for a given core n at an optical wavelength λ, can be expanded as

$$\tau_n(\lambda) = \tau_n(\lambda_0) + D_n(\lambda - \lambda_0) + \frac{S_n}{2}(\lambda - \lambda_0)^2, \quad (1)$$

where D_n and S_n represent, respectively, the chromatic dispersion and the dispersion slope for core n at the anchor wavelength, λ_0. For a MCF to function as a sample TTDL in the space diversity regime, it must fulfil two basic requirements. First, each core must feature an independent group delay at a given optical wavelength, such that the difference in group delay between successive cores, named as basic differential group delay, $\Delta\tau$, is common to all cores [7], as shown in Fig. 1. Secondly, tunability of the TTDL with the optical wavelength requires that the differential chromatic dispersion between consecutive cores, $\Delta D = D_{n+1} - D_n$, must also be common to all cores [7]. The

expression for the differential group delay between cores n and $n + 1$ is then derived from (1) as [7]:

$$\Delta\tau_{n,n+1}(\lambda) = \Delta\tau(\lambda_0) + \Delta D(\lambda - \lambda_0) + \frac{S_{n+1} - S_n}{2}(\lambda - \lambda_0)^2, \quad (2)$$

where $\Delta\tau(\lambda_0) = \tau_{n+1}(\lambda_0) - \tau_n(\lambda_0)$ is the differential group delay at the anchor wavelength.

In the wavelength diversity regime, the differential group delay is created between adjacent wavelengths, as shown in Fig. 1(b) for core n and optical sources m and $m + 1$, with wavelength spacing $\delta\lambda = \lambda_{m+1} - \lambda_m$. The differential group delay between wavelengths λ_m and λ_{m+1} is obtained from (1) as [7]:

$$\Delta\tau_n(\lambda_{m,m+1}) = D_n\delta\lambda + S_n(\lambda_1 - \lambda_0)\delta\lambda + \frac{S_n(2m-1)}{2}\delta\lambda^2. \quad (3)$$

In both operation regimes, the PCF must be optimized in terms of high-order dispersion as much as possible to offer linear tunability in a broad optical wavelength range. In fact, for satisfactory performance as a TTDL, we can assume a maximum relative error in the basic differential delay of 5% [10]. The relative error in space diversity regime between cores n and $n + 1$ as a consequence of high-order dispersion is calculated from (2) as [10]:

$$\Delta\tau_{n,n+1}(\lambda)|_{rel\_err} = \frac{S_{n+1} - S_n}{2\Delta D}(\lambda - \lambda_0). \quad (4)$$

The relative error in the wavelength diversity regime, for a given core n fed by an array of M different optical wavelengths, ($m = 1, 2, \ldots M$), is given from (3) as [10]:

$$\Delta\tau(\lambda_m, \lambda_{m+1})|_{rel\_err} = \frac{S_n}{D_n}\left[(\lambda_1 - \lambda_0) + \frac{(2m-1)}{2}\delta\lambda\right]. \quad (5)$$

Moreover, we must keep in mind that in both regimes the smaller the basic differential delay the higher is the radiofrequency processing range of the MWP signal processing functionality built upon the TTDL [7]. Apart from the above mentioned specific TTDL conditions, all the cores are required to be single-mode and should exhibit linear propagation, minimal inter-core crosstalk and maximum robustness against fiber bends and twists. In addition, the physical parameters of the cores must be distinct enough from each other such that they lie within manufacturing capabilities.

B. PCF Design

The design of the multicore PCF involves tailoring the chromatic dispersion and group delay of individual cores while keeping other propagation characteristics such as losses, nonlinearity, inter-core crosstalk and single-mode behavior within tolerable limits. The behavior of a PCF is characterized by the number of rings of airholes, x, the airhole diameter for each ring, d_1, $d_2, \ldots d_x$, the separation or pitch between airholes, δ, and the wavelength of operation [24].

Fig. 2(a) shows the schematic cross-section area of the designed 19-core silica PCF where we can see that each core is surrounded by 5 rings of airholes. It also shows the arrangement of 19 cores, each centered at the intersections of regular triangular lattice to facilitate fanout incorporation. Fig. 2(b) depicts in detail the structure of core 19 with relevant geometrical parameters. We used finite element method (FEM) software to compute different propagation characteristics at a fixed wavelength of 1550 nm, which is taken as the anchor wavelength, λ_0.

The PCF parameters were varied in a three-level hierarchy comprising x, d and δ, respectively. At the top level of the hierarchy, x is varied between 2 and 5, with the dispersion behavior largely affected by the first three rings in the short-wavelength limit, while the outer rings help to control losses by increasing the total air fraction [20]. At the second level of hierarchy, where x is fixed, d_1 for each ring is varied such that d_1/δ spans a range of 0.15 to 0.5, the upper and lower values representing the limits of single-mode confinement [13], [21]. For the rest of the rings, d/δ goes up to maximal value of 0.9. To vary the airhole diameter of each ring, we use the strategy given in [20], which enables us to evaluate a broad range of PCF structures with variable-sized airhole rings. Finally, at the third level of hierarchy, where x and d for each ring are fixed, δ is varied such that the λ_0/δ lies in the range of 0.1 to 0.9; low limit corresponding to large size and low index contrast and upper limit with smaller effective areas [22]. This analysis leads us to the design parameters for a 19-core PCF, which effectively meets the requirements set out in Section II A.

Each core of this design comprises a basic 5-ring PCF structure (similar to one reported in [23]) such that: $d_1 = d_2 = d_3$ (here in referred to as inner rings) and $d_4 = d_5$ (here in referred to as outer rings), as shown in Fig. 2(b). While the basic structure for each core of our design remains the same, as can be seen in Fig. 2(a), δ increases as we move from core 1 to 19, while, d/δ for each core also varies such that inner and outer rings increase or decrease in a fixed ratio ($d_1 = 0.36 \, d_5$).
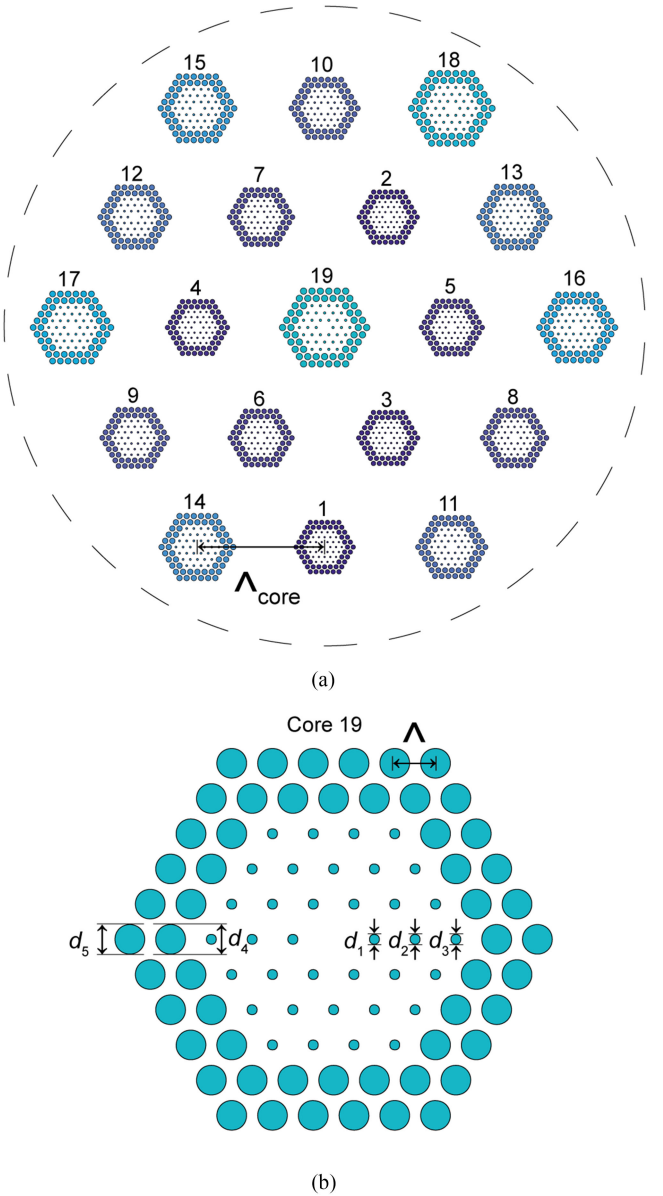

(a)

(b)

Fig. 2. Schematic cross-section view of: (a) the 19-core PCF with $\Lambda_{core} = 36 \, \mu$m that gives a cladding diameter of $\sim$250 μm (dashed line is for visualization purposes, does not reflect the outer diameter of the MCF); (b) Close-up of core 19, $d_1 = d_2 = d_3 = 0.87 \, \mu$m, $d_4 = d_5 = 2.42 \, \mu$m and $\Lambda = 3.08 \, \mu$m.

The rationale for the proposed design can be understood by looking at Fig. 3, which shows a color-coded contour plot of chromatic dispersion (black thin lines) and group delay (red thick lines) at λ_0 in which horizontal axis shows the sweep of δ and vertical axis shows the sweep of d/δ for inner rings, outer ones changing in fixed ratio to the inner. We can see that a change in δ between 2.1 to 3.3 μm translates to a broad range of chromatic dispersion from below-zero all the way up to 35 ps/nm·km. Moreover, we anticipate the high-order dispersion to be near-zero for this range of δ and d/δ considering our analysis as well as the reported flat-dispersion designs [18]–[20], [24]–[27], [23]. Therefore, in order to get constant increments in D for successive cores, δ values can be picked from this range,
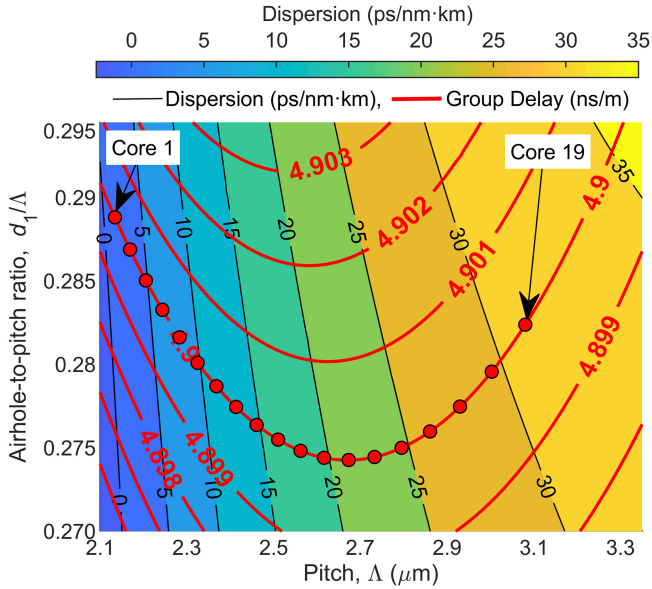
Fig. 3.   Contour plot showing chromatic dispersion (black thin lines) and group delay (red thick lines) for a 5-ring structure as a function of δ and $d_1/δ$. By changing both parameters simultaneously, 19 cores with constant $τ(λ_0)$ covering a broad dispersion range are possible, as marked by red circles.

TABLE I
PCF DESIGN PARAMETERS AND PROPERTIES

Core n	Pitch, Λ (μm)	$d/Λ$ (ring 1 -3)	$d/Λ$ (ring 4 − 5)	Dispersion D (ps/nm·km)
1	2.13	0.2888	0.8023	1.50
2	2.17	0.2869	0.7969	3.15
3	2.21	0.2850	0.7918	4.80
4	2.24	0.2833	0.7869	6.45
5	2.28	0.2816	0.7823	8.10
6	2.32	0.2801	0.7780	9.75
7	2.37	0.2787	0.7741	11.40
8	2.41	0.2774	0.7707	13.05
9	2.46	0.2764	0.7677	14.70
10	2.51	0.2755	0.7652	16.35
11	2.56	0.2748	0.7634	18.00
12	2.62	0.2744	0.7622	19.65
13	2.67	0.2743	0.7618	21.30
14	2.73	0.2744	0.7624	22.95
15	2.80	0.2750	0.7639	24.60
16	2.86	0.2760	0.7666	26.25
17	2.93	0.2775	0.7707	27.90
18	3.00	0.2796	0.7766	29.55
19	3.08	0.2824	0.7844	31.20

PCF design parameters and chromatic dispersion for each core. The group delay at the anchor wavelength $τ(λ_0)$ = 4.9 ns/m is constant for all cores.

depending on the $ΔD$ and range of dispersion required. Also, in order to fulfill the condition of constant group delay at the anchor wavelength $τ(λ_0)$ for all cores, we must stay on one of the contour lines of $τ$. Hence, $d_1/δ$ is changed on the vertical axis to keep $τ(λ_0)$ constant, corresponding to the δ value chosen on horizontal axis.

The final values of δ and $d/δ$ depend on the application scenario envisioned for the TTDL. For the proposed design, in order to get a microwave signal processing range from 1 up to 60 GHz for a 10-km link, we need a D range between 1.5 and 31.2 ps/nm·km with $ΔD$ = 1.65 ps/nm·km for a 19-sample TTDL. Each core is defined by the respective values of δ and $d/δ$ that we have marked by red circles in Fig. 3. We can also see that these values lie on the contour line corresponding to $τ(λ_0)$ = 4.9 ns/m. The value of $τ(λ_0)$ being the one that gives us a relatively broad spread in terms of δ, to aid in fiber manufacturing, while optimizing the confinement and coupling losses. The individual values of these parameters are given in Table I. Taking into account the dimensions of each individual core and with the premise of keeping mechanical reliability for bending, we assume core pitch, $Λ_{core}$ (separation between cores) in the range from 35 to 40 μm, what translates into a cladding diameter in the range from 245 to 280 μm.

III. PERFORMANCE EVALUATION

We analyze the performance of the 19-core PCF design as a tunable delay line. First, we evaluate the behavior of the group delay and chromatic dispersion to see if the conditions for TTDL functionality are fulfilled. Then, we evaluate high-order dispersion effects to see the operation wavelength range over which the TTDL performance remains satisfactory. This is followed by an analysis of the signal processing range of the TTDL

when applied to microwave signal filtering. Finally, we discuss intercore crosstalk and fiber nonlinear response.

A. TTDL Operability

Fig. 4 plots the main propagation characteristics for each core, enabling us to get an overview of the TTDL performance over a broad wavelength range between 1.5 and 1.6 μm.

Fig. 4(a) shows the differential group delay per unit length where we can appreciate, first, that the condition of common group delay at the anchor wavelength is fulfilled by all the cores as $Δτ$ is zero at 1550 nm. Second, we can see that the differential group delay increases linearly as the optical wavelength increases, always keeping the same value between all adjacent cores at a given wavelength. When we operate in space diversity, the basic differential delay $Δτ$ ranges approximately from 16.5 (starting at 1551 nm) up to 825 ps (at 1600 nm). These values translate into a radiofrequency processing range (given by the inverse of $Δτ$) from 1.21 up to 60.60 GHz. If we operate in wavelength diversity considering $δλ$ = 1 nm, the basic differential delay spans from 15 (core 1) up to 312 ps (core 19), resulting in a radiofrequency processing range from 3.21 up to 66.70 GHz. For the particular application of microwave signal filtering, which we will evaluate later, the radiofrequency processing range corresponds to the filter Free Spectral Range (FSR) or spectral periodicity.

Fig. 4(b) plots the chromatic dispersion D showing that the second condition of constant $ΔD$ between consecutive cores is fulfilled strictly over a broad wavelength range for most of the cores (1 to 15), while for the larger cores (15 to 19) is fulfilled over a wavelength range of approximately 40 nm around $λ_0$. This is because the dispersion slope S, shown in Fig. 4(c), increases with the core number, as δ increases. Nonetheless, we consider the maximum value of S, around 0.035 ps/nm²·km, very small to represent a source of considerable error, as explained below.
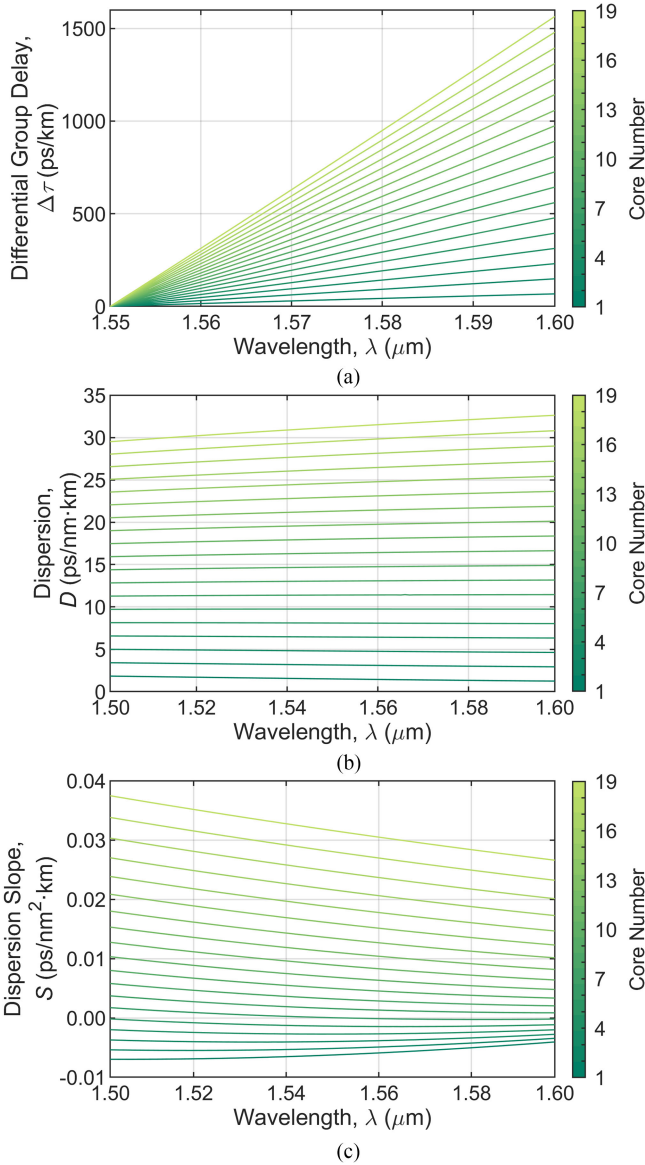
Fig. 4. Propagation characteristics of the 19 cores as a function of the wavelength. (a) Differential Group Delay $\Delta\tau$, which is constant between any pair of cores at a given wavelength; (b) Chromatic Dispersion D, which exhibits a constant increment between consecutive cores (ΔD) over a broad wavelength range and (c) Dispersion Slope S, which is near-zero for all cores.
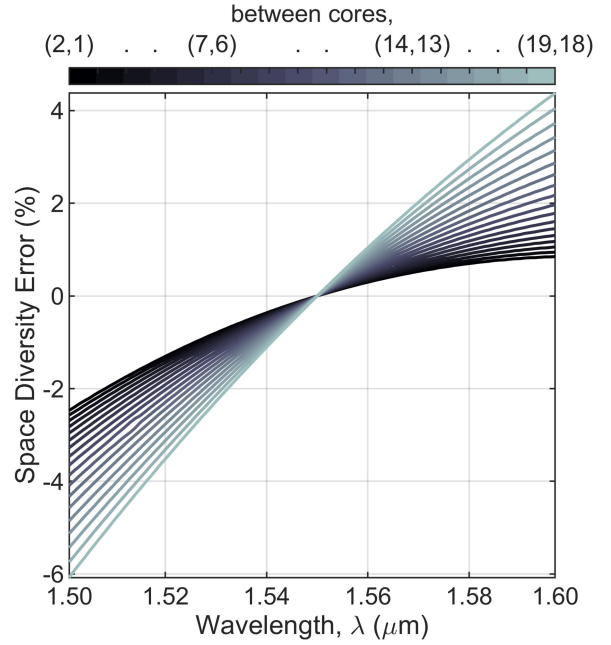

Fig. 5. Space-diversity relative error (%) between consecutive cores as a function of the optical wavelength, given by (4).
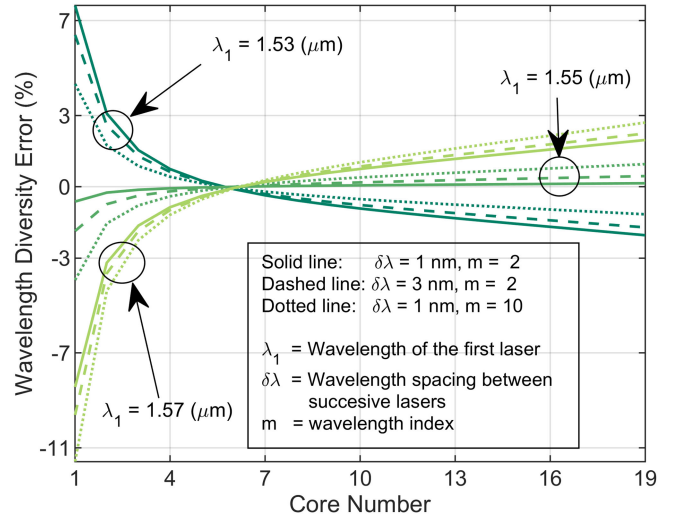

Fig. 6. Wavelength-diversity error (%) as a function of the core number, given by (5), for different conditions of the input optical wavelength array. λ_1 = initial wavelength, m: wavelength index, $\delta\lambda$: wavelength spacing, ($m = 1, 2, \ldots M$, $\lambda_m = \lambda_1 + (m-1)\delta\lambda$).

We evaluate in Fig. 5 the relative error given by (4) in terms of high-order dispersion for the space-diversity regime, which depends on the ratio $\Delta S/\Delta D$ and the operation wavelength. In Figs. 4(b) and (c), we saw that as the wavelength increases, ΔD increases slightly while ΔS decreases. As a consequence, the relative error increases as we move apart from the anchor wavelength at 1550 nm, as shown in Fig. 5. All in all, we can see that the overall error remains below 6% over a very broad wavelength range of $\lambda_0 \pm 50$ nm. This will result, as we stated before, in a broad TTDL radiofrequency processing range up to 60.60 GHz.

Fig. 6 shows the relative error as a function of each core when we operate in the wavelength-diversity regime for different conditions of the optical wavelength input array comprising M wavelengths. We selected three different values for the initial optical wavelength, λ_1: light green lines correspond to $\lambda_1 = 1570$ nm; medium green lines to $\lambda_1 = 1550$ nm (i.e., the reference wavelength λ_0) and dark green lines to $\lambda_1 = 1530$ nm. For each initial wavelength, we compared 3 different situations where we vary the wavelength spacing $\delta\lambda$ and the position of the specific optical wavelength into the array m ($m = 1, 2, \ldots M$), which we call wavelength index. For the sake of clarity, we must keep in mind that $\lambda_m = \lambda_1 + (m-1)\delta\lambda$.

Generally, the first three cores perform worse than the rest for which the errors stay within 5% over the 40-nm wavelength range. This can be explained by the relatively high ratio of S/D for the initial cores since D is very small. Referring to Figs. 4(b) and (c), we can see that S and D follow opposite trends with increasing wavelengths, what results in relatively worse performance at smaller wavelengths. As for the effect of increasing m or $\delta\lambda$, we see in Fig. 6 that: for relatively smaller wavelengths such that $\lambda_1 < \lambda_0$ (dark green lines showing the case in which $\lambda_1 = 1.53~\mu$m), the error decreases with the increase in m or $\delta\lambda$. Whereas, as we reach the anchor wavelength for $\lambda_1 = \lambda_0$ (medium green lines) and beyond where $\lambda_1 > \lambda_0$ (light green lines showing the case in which $\lambda_1 = 1.57~\mu$m), the error now increases. Interestingly, Core 6 has a near-zero dispersion slope S due to which it has almost zero error for all cases. All in all, the error remains low for most of the cores over a broad wavelength range, enabling tunability of the TTDL with a radiofrequency processing range, as stated before, up to 66.70 GHz.

Finally, we apply the proposed TTDL to a representative microwave photonic application of tunable signal filtering in both space- and wavelength-diversity regimes for a 10-km link. The RF filtering effect is produced when we combine in the optical domain all the TTDL samples at the PCF output and detect them using a single photodetector [1]. The spectral periodicity or FSR of the microwave filter is then given by the inverse of the differential basic delay, i.e., FSR $= 1/\Delta\tau$. Fig. 7(a) shows the frequency response of the 19-tap RF filter in space diversity for two extreme cases of wavelength of operation. In one case, we operate the TTDL at a wavelength of 1551 nm, with only 1-nm separation from λ_0, giving a maximal FSR of 60.6 GHz. While, in the second case, a wavelength of 1560 nm is used to get an FSR of 6.0 GHz. Fig. 7(b) shows the frequency response of a 10-tap RF filter implemented with the same 19-core PCF when we feed the delay line by an array of 10 lasers and exploit the wavelength-diversity regime. We compare here the FSR obtained from the TTDL implemented on core 1 and 19, assuming a wavelength spacing between lasers of 1 nm. Core 1, which exhibits the lowest dispersion, features the highest FSR of 66.7 GHz, while core 19, which exhibits the highest dispersion, provides the minimal value of FSR at 3.2 GHz. Thus, the tunability of the filter covers the entire microwave region making it suitable for a broad range of microwave applications.

B. Intercore Crosstalk

Intercore crosstalk is calculated by using the expressions of average power coupling coefficient h_{mn} between cores m and n at a distance between cores, $\Lambda_{core} = 36~\mu$m, using the expression given in [28], that takes into account the effects of bends and twists. The mode-coupling coefficient κ_{mn}, which is required as input to the expression of h_{mn}, is calculated semi-analytically by directly extracting the electric field values from the FEM solver. Correlation length is assumed to be 50 mm [28].

Table II provides the range of different core propagation characteristics, where we can see that the minimum index contrast between core and cladding Δn corresponds to core 19.
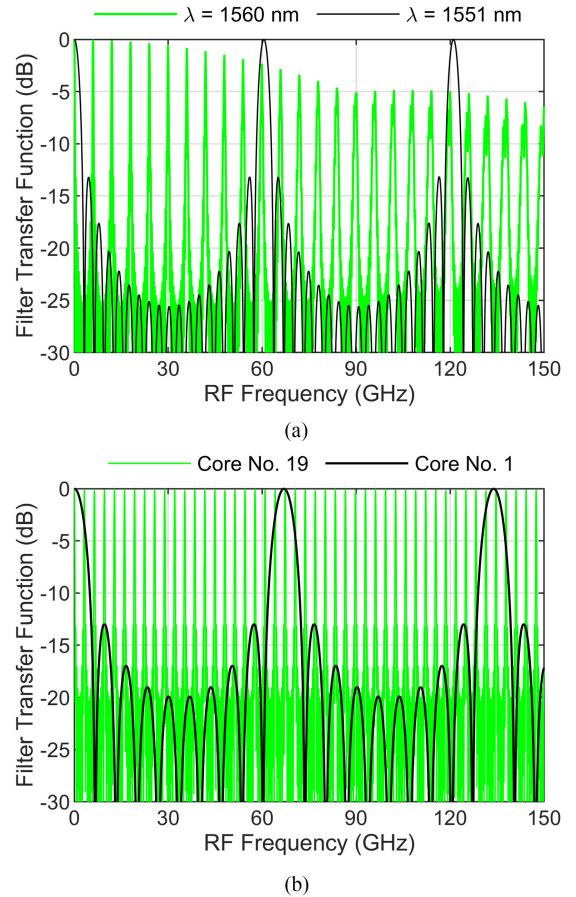

(a)

(b)

Fig. 7. Comparison of the transfer function of a microwave signal filter based on the proposed TTDL for a 10-km link while operating in: (a) Space-diversity regime, (b) wavelength-diversity regime.

TABLE II
PROPERTIES OF CORES

Property	Core 1	Core 19
Effective Area (μm^2)	22.4	29.7
Index Contrast (%)	1.52	0.34
Confinement Loss (dB/km)	2.4e-3	1.1e-5
Nonlinearity Index(1/W.km)	4.1	3.9

The corresponding characteristics (not shown) for cores 2 to 18 lie between those of cores 1 and 19.

Furthermore, we show in Fig. 8 the effective index difference between consecutive pairs of cores, Δn_{eff}, computed at $\lambda = 1550$ nm. We can see Δn_{eff} decreases for cores with higher core number, being cores (18, 19) the worst theoretical case since the crosstalk is inversely proportional to both Δn and Δn_{eff}, [28]. Hence, we arrange the cores with lower Δn_{eff} to be far apart from each other. After this arrangement, in the final layout shown in Fig. 2(a), the worst case in terms of effective index difference between adjacent cores can be easily assessed as being cores 16 and 13. We must note, therefore, that other pairs of cores with similar or lower effective index difference will not produce a higher crosstalk because they are not placed in adjacent positions in the cross-sectional area of the fiber. Thus, we evaluate the fiber
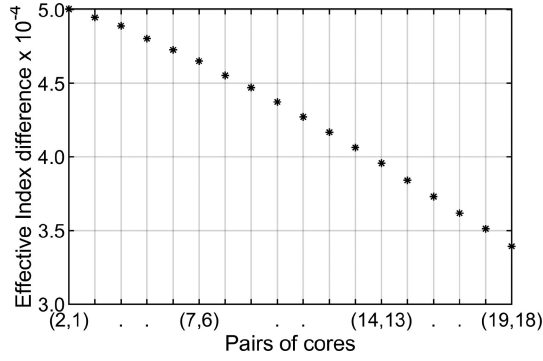
Fig. 8. Difference in effective indices, Δn_{eff}, between consecutively numbered pairs of cores, computed at $\lambda = 1550$ nm.
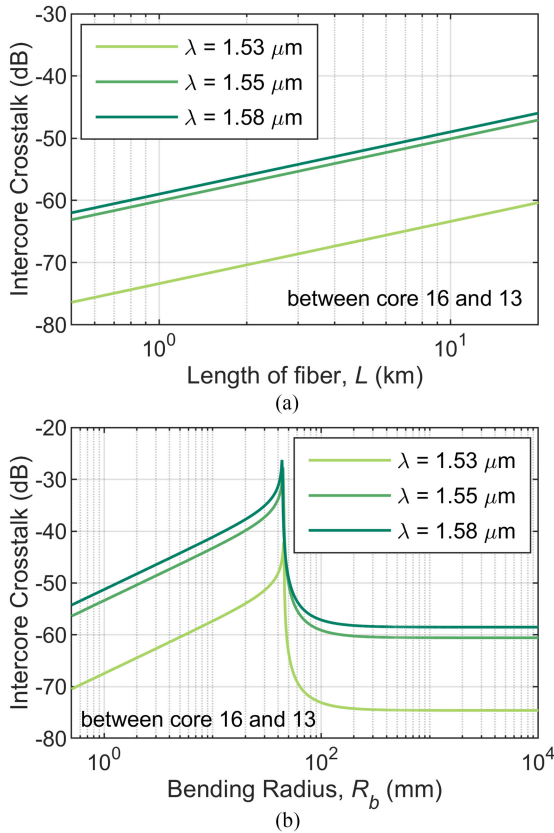

Fig. 9. Crosstalk experienced between cores 16 and 13 at $\lambda = 1.53$ μm, 1.55 μm and 1.58 μm, as a function of: (a) fiber length for $R_b = 50$ mm, (b) fiber bending radius for $L = 10$ km.
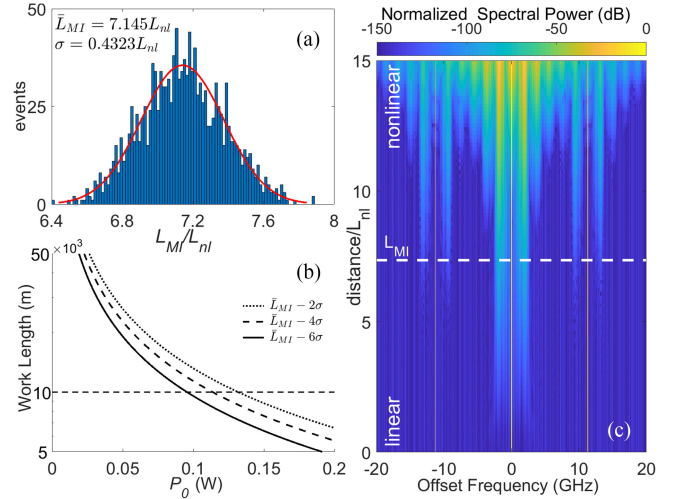

Fig. 10. (a) Histogram illustrating the distance at which MI sets in for 1400 runs (blue), fitted to a normal distribution (red) with mean length $\bar{L}_{MI}$ and standard deviation σ (see labels). (b) Work length versus input optical power P_0 defined at -2σ, -4σ and -6σ (dotted, dashed, and solid lines respectively). The horizontal dashed line represents the 10 km of fiber length. (c) Typical spectral evolution of the RF-modulated optical signal in core 1 at a modulating frequency of 11.2 GHz, showing that the nonlinear regime appears only after a length of $7.35L_{nl}$ (equivalent to 1544.6 km for $P_0 = 1$ mW and $\gamma = 0.0048$ (W.m)$^{-1}$).

intercore crosstalk and its sensitivity against fiber curvatures for the pair of cores 16 and 13.

Fig. 9(a) shows the intercore crosstalk between cores 16 and 13 as a function of the link length, L, for three different wavelengths, $\lambda = 1.53$ μm (light green lines), 1.55 μm (medium green lines) and 1.58 μm (dark green lines). We appreciate a crosstalk level of -50.1 dB after 10 km at the anchor wavelength of 1.55 μm, whereas, at $\lambda = 1.53$ μm and 1.58 μm, it is -63.4 dB and -49.0 dB, respectively. Fig. 9(b) shows the intercore crosstalk as a function of the fiber bending radius R_b

for the same pair of cores, $L = 10$ km, and the same wavelengths. The trend for wavelength is the same as Fig. 9(a), signifying better performance in terms of crosstalk at lower wavelengths. Moreover, we see that at the phase-matching condition between cores, we get a peak value of crosstalk of -27.7 dB at the anchor wavelength. This corresponds to the threshold bending radius for the proposed fiber layout in Fig. 2(a), that is, $R_{pk} = 44.75$ mm [29]. At $\lambda = 1.53$ μm and 1.58 μm, the peak value of crosstalk is -42.1 dB and -26.2 dB, respectively.

All in all, that value of crosstalk can be considered low enough to not represent a problem across the length of the fiber link. Moreover, as shown in Fig. 2(a), we have arranged the cores within the fiber cross-sectional area as to place dissimilar ones in terms of effective index next to each other to reduce the crosstalk further.

C. Fiber Nonlinear Response Analysis

The aim of this section is to demonstrate that all fiber cores behave linearly for a 10-km link in the power range relevant for microwave photonics applications (around 1 mW). In this context, linear means that none of the noise frequencies exhibits a normalized spectral power beyond a threshold set to -80 dB. In effect, the process behind the growth of noise frequencies is modulation instability (MI). Since MI is a stochastic process, we have run 1400 propagation simulations using the nonlinear Schrodinger equation for optical fibers [30], neglecting fiber losses, initiated with different noise seeds. The normal distribution in Fig. 10(a) shows the length at which our fiber satisfies the above criterion. We called this length modulation instability length L_{MI}, which is shown in units of the nonlinear length, $L_{nl} = 1/(\gamma P_0)$. To ensure linear signal propagation in
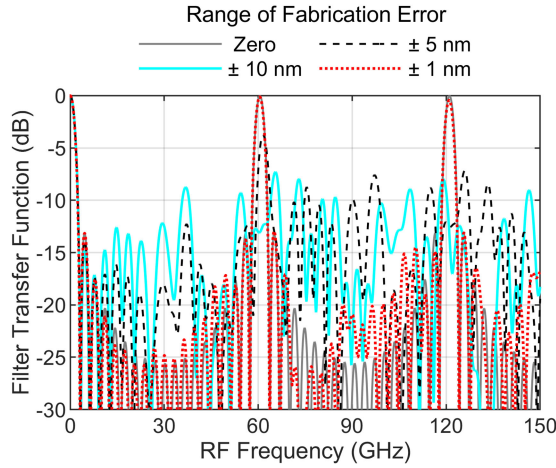
Fig. 11. Random fabrication errors in the range of ± 10, ± 5 and ± 1 nm added to design values of airhole diameter and pitch reflect in the transfer function of a microwave signal filter based on the proposed TTDL for a 10-km link operating at $\lambda = 1551$ nm in the space-diversity regime.

all cores, we modelled the propagation of microwave photonic signals for the worst-case scenario. This case is represented by the core 1 that features the highest non-linearity index: $\gamma = 0.0048$ (W.m)$^{-1}$.

We define the fiber link *work length*, i.e., the fiber length at which nonlinear effects are statistically insignificant, a few standard deviations, σ, below $\bar{L}_{MI}$. In Fig. 10(b), we show the work length in physical units in relation to P_0 for -2σ, -4σ, and -6σ. The horizontal dashed line represents the proposed fiber link length of 10 km for the given P_0 and γ. We see that the fiber design presented in this paper will operate in the linear regime according to the established criterion and for input optical powers P_0 on the order of 100 mW.

Fig. 10(c) shows a particular case, from the 1400 simulation runs, of the evolution in which we can appreciate the transition between the linear and nonlinear regimes. The horizontal white dashed line marks the length 7.35 L_{nl} (equivalent to 1544.6 km for $P_0 = 1$ mW and the γ mentioned above) at which the normalized spectral power of the new frequencies generated, caused by the nonlinear effects, reaches -80 dB.

IV. DISCUSSION

In our design, variations on the airhole and pitch values would have a direct impact on the overall TTDL performance. Here we discuss the impact of fluctuations in the design values due to potential random fabrication errors on the performance of a TTDL in the space- and wavelength-diversity regimes for the representative case of a microwave signal filter. We must note that final fabrication errors cannot be predicted with full certainty because the actual dimensions will fluctuate across the length of the fiber during a realistic drawing process. This may serve to average out the errors to our advantage and can only be ascertained by fabricating the fiber and testing its performance as a delay line.
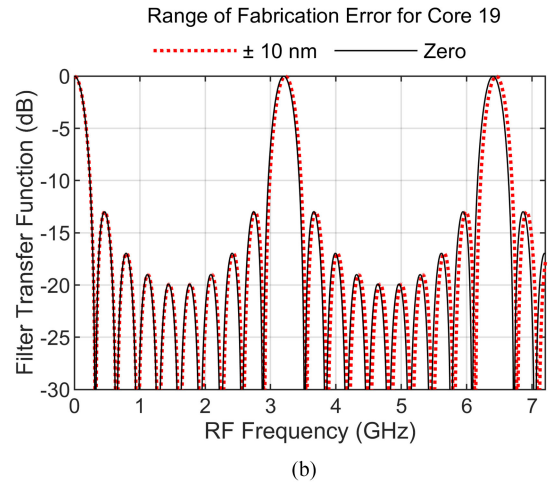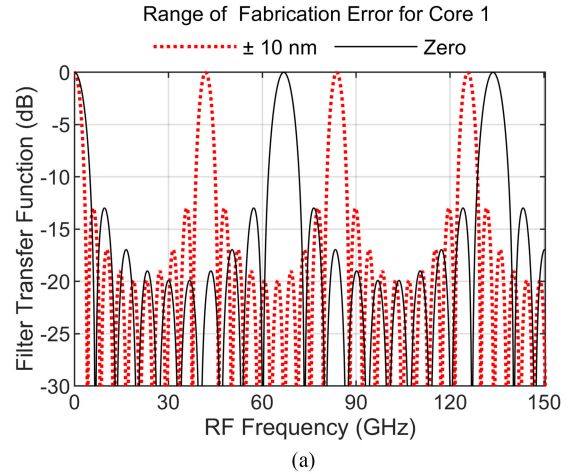

(a)

(b)

Fig. 12. Random fabrication error in the range of ± 10 nm added to design values of airhole diameter and pitch reflect in the transfer function of a microwave signal filter based on the proposed TTDL for a 10-km link operating at $\lambda = 1550$ nm with $d\lambda = 1$ nm in the wavelength-diversity regime.

Fig. 11 shows the filter transfer function when operating in space diversity for three cases in which we randomly fluctuate airhole diameter and pitch values for each core in the range of ± 10, ± 5 and ± 1 nm around the design values and a fourth case showing the ideal design. We can see that when the fluctuations are ± 10 nm (solid cyan line), the filter transfer function is distorted completely for the second resonance. For an error ranging ± 5 nm around the design values (dashed black line), the situation is somewhat better as the second resonance is above -5 dB. Finally, if the error can be brought in the range of ± 1 nm (red dotted line), we can have an almost ideal TTDL, with similar levels for the main resonances and a high value of main to secondary side-lobe (MSSL) ratio.

Effect of fabrication errors on wavelength-diversity operation for the worst case given by maximum tolerances of ± 10 nm is evaluated in Fig. 12. Here, only the absolute values of S and D in each core are of significance for the filter transfer function. Thus, to the extent that fabrication errors change the value of these parameters for a given core, only the FSR of the filter will be affected, compressing or stretching the filter

response. Maximum variation will be given in core 1, as shown in Fig. 12(a), where the FSR is reduced from its ideal value (black solid line) to 41.8 GHz (red dotted line) as D increases from the ideal 1.5 to 2.4 ps/nm·km. In Fig. 12(b), we show the minimum alteration of FSR, which occurs for core 19, where D is slightly reduced from 31.2 down to 30.9 ps/nm·km.

To appreciate the fabrication challenge posed by this design, consider that each core features two different d/δ values, since the airhole diameters for inner rings and outer rings are different. To get a certain value of pitch, this 5-ring core preform is scaled down at the intermediate stage of drawing a cane. Thus, we need 19 different core preforms for the proposed design, which could result quite challenging since each preform could present a certain manufacturing error in initial capillary sizes. We discuss a few approaches to address this challenge.

In the first approach, we start with a single preform (instead of 19 different preforms) and scale it in size to serially draw 19 different canes (with distinct δ values), which can subsequently be stacked together to draw the final multicore fiber. This approach can take two different directions. First, if one could apply different gas pressure to each air hole size during the final draw stage, the airholes would inflate or collapse accordingly, thus changing the d/δ values. This would require 38 different pressure controls (one for each airhole size). However, in current fiber manufacturing facilities, the available number of pressure controls is lower.

Alternatively, we could use the same pressure for all cores, i.e., the standard one used to keep the holes from collapsing under surface tension. In this scheme, we would have the same value of d/δ for all cores. What this means for the TTDL is that group delay would no longer be constant at the anchor wavelength, i.e., the group delay would not follow the same red contour line as plotted in Fig 3. However, the incremental dispersion values would remain as required, so tunability with the optical wavelength would be guaranteed. Group delay could then be compensated externally by adding a fiber segment with a certain length to each core, as part of the fan-in/fan-out. It will be the focus of future work to fabricate the latter version as an initial step to see how well fabrication errors can be controlled.

V. CONCLUSION

We have presented, for the first time to our knowledge, the design of a 19-sample tunable TTDL for radiofrequency signals using a multicore PCF. To allow TTDL operation, the PCF comprises 19 different cores where each core features an independent and incremental value for both the group delay and chromatic dispersion while providing low confinement losses, low crosstalk and linear operation. As compared to other SDM optical fiber technologies, this PCF offers higher design flexibility and better performance since it is possible to change the chromatic dispersion over a broad range from zero up to around 35 ps/km·nm while keeping the dispersion slope negligible using a 5-ring PCF structure for all the cores. For comparison, dispersion range of a recently reported TTDL based on a 7-core heterogeneous solid-core fiber is 14.3 to 20.3 ps/nm·km, [31]. As a result, a tunable TTDL for microwave signal processing with

a broad radiofrequency processing range (from 1 to 67 GHz) is possible, at least theoretically, in both space- and wavelength-diversity regimes for a link length of 10 km.

The design and analysis presented here has important implications for MWP applications since it opens the way to increasing both the number of samples and the radiofrequency processing range of a TTDL based on SDM technology in a single optical fiber. This tunable TTDL can be applied to a variety of radiofrequency signal processing applications, such as signal filtering, optical beamforming for phased array antennas, multi-cavity optoelectronic oscillation or arbitrary waveform shaping. Beyond MWP, this approach can be extended to additional electrical or optical signal processing applications that require a given set of group delay or chromatic dispersion values.

REFERENCES

[1] J. Capmany, J. Mora, I. Gasulla, J. Sancho, J. Lloret, and S. Sales, "Microw. photon. signal processing," *J. Lightw. Technol.*, vol. 31, no. 4, pp. 571–586, Feb. 2013.

[2] K. Wilner and A. P. van den Heuvel, "Fiber-optic delay lines for microwave signal processing," *Proc. IEEE*, vol. 64, no. 5, pp. 805–807, May 1976.

[3] J. Capmany, D. Pastor, and B. Ortega, "New and flexible fiber-optic delay-line filters using chirped Bragg gratings and laser arrays," *IEEE Trans. Microw. Theory Techn.*, vol. 47, no. 7, pp. 1321–1326, Jul. 1999.

[4] D. B. Hunter and R. A. Minasian, "Microwave optical filters using in-fiber Bragg grating arrays," *IEEE Microw. Guided Wave Lett.*, vol. 6, no. 2, pp. 103–105, Feb. 1996.

[5] A. Loayssa and F. J. Lahoz, "Broad-band RF photonic phase shifter based on stimulated Brillouin scattering and single-sideband modulation," *IEEE Photon. Technol. Lett.*, vol. 18, no. 1, pp. 208–210, Jan. 2006.

[6] D. J. Richardson, J. M. Fini, and L. E. Nelson, "Space-division multiplexing in optical fibers," *Nature Photon.*, vol. 7, no. 5, pp. 354–362, May 2013.

[7] I. Gasulla and J. Capmany, "Microwave photonics applications of multi-core fibers," *IEEE Photon. J.*, vol. 4, no. 3, pp. 877–888, Jun. 2012.

[8] I. Gasulla, D. Barrera, J. Hervás, and S. Sales, "Selective grating inscription in multicore fibers for radiofrequency signal processing," in *Proc. Opt. Fiber Commun. Conf.*, Los Angeles, California, 2017, Paper. W4B.6.

[9] S. Garcia and I. Gasulla, "Design of heterogeneous multicore fibers as sampled true-time delay lines," *Opt. Lett.*, vol. 40, no. 4, pp. 621–624, Feb. 2015.

[10] S. García and I. Gasulla, "Dispersion-engineered multicore fibers for distributed radiofrequency signal processing," *Opt. Express*, vol. 24, no. 18, pp. 153–156, Sep. 2016.

[11] R. Guillem, S. García, J. Madrigal, D. Barrera, and I. Gasulla, "Few-mode fiber true time delay lines for distributed radiofrequency signal processing," *Opt. Express*, vol. 26, no. 20, pp. 25761–25768, Oct. 2018.

[12] S. García, D. Barrera, J. Hervás, S. Sales, and I. Gasulla, "Microwave signal processing over multicore fiber," *Photonics.*, vol. 4, no. 4, pp. 1–14, Dec. 2017.

[13] J. C. Knight, T. A. Birks, P. St. J. Russell, and D. M. Atkin, "All-silica single-mode optical fiber with photonic crystal cladding," *Opt. Lett.*, vol. 21, no. 19, pp. 1547–1549, Oct. 1996.

[14] P. Russell, "Photonic crystal fiber: finding the holey grail," *Opt. Photon. News*, vol. 18, no. 7, pp. 26–31, Jul. 2007.

[15] P. S. J. Russell, "Photonic crystal fibers: Basics and applications," in *Optical Fiber Telecommunications*, 5th ed., I. P. Kaminow, T. Li, and A. E. Willner, Eds. New York, NY, USA: Academic Press, 2008, pp. 485–522.

[16] J. C. Knight, T. A. Birks, B. J. Mangan, P. St. J. Russel, G. G. Vienne, and J.-P. De Sandro, "Multicore photonic crystal fibers," in *Proc. 12th Int. Conf. on. Opt. Fiber Sensors*, Williamsburg, Virginia,1997, Paper. PDP5.

[17] P. Russell, "Photonic Crystal Fibers: A Historical Account," *IEEE LEOS Newslett.*, vol. 5, no. 21, pp. 11–15, Oct. 2007.

[18] A. Ferrando, E. Silvestre, J. J. Miret, and P. Andrés, "Nearly zero ultra-flattened dispersion in photonic crystal fibers," *Opt. Lett.*, vol. 25, no. 11, pp. 790–792, Jun. 2000.

[19] W. Reeves, J. Knight, P. Russell, and P. Roberts, "Demonstration of ultra-flattened dispersion in photonic crystal fibers," *Opt. Express*, vol. 10, no. 14, pp. 609–613, Jul. 2002.

[20] K. Saitoh, M. Koshiba, T. Hasegawa, and E. Sasaoka, "Chromatic dispersion control in photonic crystal fibers: Application to ultra-flattened dispersion," *Opt. Express*, vol. 11, no. 8, pp. 843–852, Apr. 2003.

[21] T. A. Birks, J. C. Knight, and P. St. J. Russell, "Endlessly single-mode photonic crystal fiber," *Opt. Lett.*, vol. 22, no. 13, pp. 961–963, Jul. 1997.

[22] N. A. Mortensen and J. R. Folkenberg, "Low-loss criterion and effective area considerations for photonic crystal fibers," *J. Opt.: A Pure Appl. Opt.*, vol. 5, no. 3, pp. 163–167, May 2003.

[23] F. Poletti, V. Finazzi, T. M. Monro, N. G. R. Broderick, V. Tse, and D. J. Richardson, "Inverse design and fabrication tolerances of ultra-flattened dispersion holey fibers," *Opt. Express*, vol. 13, no. 10, pp. 3728–3736, 2005.

[24] K. P. Hansen *et al.*, "Highly nonlinear photonic crystal fiber with zero-dispersion at 1.55 μm," in *Proc. Opt. Fiber Commun. Conf. and. Exhib.*, 2002, Paper FA9.

[25] F. Poli, A. Cucinotta, S. Selleri, and A. H. Bouk, "Tailoring of flattened dispersion in highly nonlinear photonic crystal fibers," *IEEE Photon. Technol. Lett.*, vol. 16, no. 4, pp. 1065–1067, Apr. 2004.

[26] T.-Lin L. Wu and C.-Hsin H. Chao, "A novel ultraflattened dispersion photonic Crystal fiber," *IEEE Photon. Technol. Lett.*, vol. 17, no. 1, pp. 67–69, Jan. 2005.

[27] T. Matsui, J. Zhou, K. Nakajima, and I. Sankawa, "Dispersion-flattened photonic crystal fiber with large effective area and low confinement loss," *J. Lightw. Technol.*, vol. 23, no. 12, pp. 4178–4183, Dec. 2005.

[28] M. Koshiba, K. Saitoh, K. Takenaga, and S. Matsuo, "Analytical expression of average power-coupling coefficients for estimating intercore crosstalk in multicore fibers," *IEEE Photon. J.*, vol. 4, no. 5, pp. 1987–1995, Oct. 2012.

[29] T. Hayashi, T. Nagashima, O. Shimakawa, T. Sasaki, and E. Sasaoka, "Crosstalk variation of multi-core fiber due to fiber bend," in *Proc. 36th Eur. Conf. Exhib. Opt. Commun.*, 2010, pp. 1–3.

[30] V. E. Zakharov and L. A. Ostrovsky, "Modulation instability: The beginning," *Physica D: Nonlinear Phenomena*, vol. 238, no. 5, pp. 540–548, 2009.

[31] S. García, M. Ureña, and I. Gasulla, "Heterogeneous multicore fiber for optical beamforming," in *Proc. 2019 Int. Topical Meeting Microw. Photon. (MWP)*, 2019, pp. 1–4.

Sabahat Shaheen received the B.E. degree in telecommunications engineering from the National University of Science and Technology, Pakistan, in 2009. She received the first level master's degree in photonic networks engineering (MAPNET), as a part of Erasmus Mundus Program, from Scuola Superiore Sant'Anna, Italy and Aston University, United Kingdom in 2016.

She worked as a Telecommunications Engineer for five years, between 2009–2014, in the corporate sector of Pakistan. Currently, she is a Doctoral Researcher with Universitat Politècnica de València, where she works on space-division multiplexing technologies for emergent fiber-wireless communications.

Itandehui Gris-Sánchez received the B.E. degree in telecommunications engineering from the National Autonomous University of México (UNAM), Mexico, in 2006. She holds a Ph.D. in physics (2012) from the University of Bath, U.K. Currently, she works with the Photonics Research Labs, Universitat Politècnica de València (UPV), developing optical fibers for their application in Microwave Photonics. As a Postdoctoral Researcher she has developed highly specialized optical fiber-based devices. She has extensive experience on the design, fabrication, postprocessing and characterization of photonic crystal fibers, multicore fibers, special index profile fibers as the Airy fiber, and photonic devices like the photonic lanterns. She has worked closely with international partners in industry and academia and her work has found applications in astrophotonics, biomedical instrumentation, and telecommunications. She is interested in exploring further the possibilities of specialty optical fibers to deliver, transform, and manipulate light.

Ivana Gasulla (Senior Member IEEE) received the M. Sc. degree in telecommunications engineering and the Ph.D. degree in telecommunications from the Universitat Politècnica de València (UPV), Spain, in 2005 and 2008, respectively. She is currently a Senior Researcher (Ramon y Cajal Fellow) and Deputy Director for dissemination and promotion with the iTEAM Research Institute, UPV. In 2016, she was awarded a prestigious ERC Consolidator Grant to develop new space-division multiplexing technologies for emergent fiber-wireless communications through the Project InnoSpace. From 2012 to 2014, she was a Fulbright Scholar at Stanford University.

Her current research interests encompass the application of multimode and multicore fibers to microwave photonics systems. The results of her work have led to more than 120 international publications, highlighting contributions to *Nature Communications* and *Nature Photonics*. She is a member of the TPC of the most prestigious conferences in the field: European Conference on Optical Communications (ECOC), Optical Fiber Communication Conference (OFC), and IEEE International Topical meeting on Microwave Photonics (MWP), among others.